**ARTICLE TYPE**

# A carbohydrate-grafted nanovesicle with activatable optical and acoustic contrasts for dual modality high performance tumor imaging

**Xuanjun Wu,[a] Bijuan Lin,[a] Mingzhu Yu,[a] Liu Yang,[a] Jiahuai Han,[b] and Shoufa Han[a],***

Activatable molecular systems enabling precise tumor localization are valuable for complete tumor resection. Herein, we report sialic acid-capped polymeric nanovesicles encapsulating near infrared profluorophore (pNIR@P@SA) for lysosome activation based dual modality tumor imaging. The probe features surface-anchored sialic acid for tumor targeting and a core of near infrared profluorophore (pNIR)
10 which undergoes lysosomal acidity triggered isomerization to give optical and optoacoustic signals upon cell internalization. Imaging studies reveal high-efficiency uptake and signal activation of pNIR@P@SA in subcutaneous tumor and millimeter-sized liver tumor foci in mice. The high tumor-to-healthy organ signal contrasts and discern of tiny liver tumors from normal liver tissues validate the potentials of pNIR@P@SA for high performance optical and optoacoustic imaging guided tumor resection.

## Introduction

15    With the increasing cancer mortality, technologies that could improve the outcome of cancer treatment are of clinical interests. Widely employed for tumor treatment, surgical resection is often hampered by limited visibility of tiny or embedded tumors,
20 leading to incomplete surgical ablation and ensuing tumor recurrence. As such, optical systems capable of guiding surgeons to evasive tumors are being vigorously explored.[1] Conventional dyes lack the specificity to recognize tumor cells. To achieve high tumor-to-healthy tissue signal contrast, dyes are often armed
25 with tumor-targeting entities which are largely confined to antibody, folate, peptides, and aptamers, etc.[2] Sialic acids (SA), a family of 9-carbon monosaccharides derived from *N*-acetyl-neuraminic acid, are typically located at termini of cell surface glycans.[3] Cell surface hypersialylation is a character of many
30 cancers and the hypoxic core of solid tumors,[4] suggesting elevated metabolic demand of SA by these tumor cells. Recently, dye-labelled SA was demonstrated for tumor detection in mice, showing the applicability of SA for *in vivo* tumor targeting.[5]

     Optical systems that are activated to fluorescence-on states
35 while remain silent at off-target settings are advantageous for high signal-to-background contrast.[1] Fluorescence imaging suffering strong photon diffusion in tissues whereas optoacoustic imaging employs weakly scattered ultrasound and thus enables deep tissue imaging.[6]. Recently two molecular systems with an
40 inert reference photoacoustic signal and another varibale optoacoustic signals responsive to MMP-2 enzyme or reactive oxygen species have been constructed for activatable photoacoustic imaging.[7] Complementing to these approaches, we herein report "turn-on" imaging based on isomerization of a
45 non-optoacoustic molecular entity into an optoacostic agent within acidic lysosomes. To integrate the advantages of NIR fluorescence imaging (low background signals) and acoustic imaging (deep tissue penetration), we herein report a SA-capped polymersome featuring NIR profluorophore (pNIR) for lysosome
50 activation based optical and optoacoustic tumor imaging (Fig. 1). pNIR@P@SA comprises SA displayed on surface of polymeric vesicles for tumor targeting, a shell of biocompatible poly[styrene-*alter*-(maleic acid)], and a hydrophobic core of pNIR responsive to lysosomal acidity. Imaging studies in tumor-
55 bearing mice intravenously injected with pNIR@P@SA reveal "turn-on" NIR fluorescence and acoustic signals in tumors and pharmacokinetics advantageous for imaging guided surgery.



60 **Fig. 1** Schematic for lysosomal acidity activation based fluorescence and optoacoustic tumor imaging with pNIR@P@SA (A). The polymeric vesicle is featured by SA anchored on the surface at C-9 for tumor targeting and encapsulated pNIR poised to proton mediated isomerization to give NIR fluorescence and
65 optoacoustic signals (B).

## Results and discussion

### Construction and characterization of pNIR@P@SA

     Oversialylation of cell surface glycoconjugates is a hallmark of a number of cancer types and the hypoxic cores of solid

tumors.[4] Cell surface SA is metabolically attached to preceding glycan acceptors by glycosidic bonds at C-2, mostly α-2,3/6 linkages.[3] Nanomedicine with targeting and therapeutic/imaging entities on a single particle has attracts enormous interests. Being ligands of endogenous SA-binding lectins, sialosides with C-2 glycosidic bonds have been integrated with various nanocarriers for biomedical applications.[8] The reported tumor imaging with fluorescein isothiocynate-labelled SA suggests that SA with appropriate substituent at C-9 could be effectively taken up by tumors from bloodstream.[5] To circumvent potential recognition of α-2,3/6- sialosides by endogenous lectins,[9] pNIR@P@SA with C-9 linked SA, an abiotic linkage potentially inert to lectins, was designed for *in vivo* tumor targeting.

Apart from targetability, probes switched to signal-on state in tumors while remaining silent at off-target settings are advantageous for low background imaging.[10] As such, rhodamine derivatives with intramolecular spirorings have been employed for tumor detection by lysosomal acidity triggered fluorogenic opening of the rings.[11] NIR dyes are superior to rhodamines for *in vivo* imaging owing to minimal autofluorescence of biological tissues in NIR window.[12] Hence pNIR, a pH responsive profluorophore with intramolecular lactam,[5b] was used as the lysosome acidity reporting element in this report. Poly[styrene-*alter*-(maleic acid)] is biocompatible as its conjugate with neocarcinostation has been clinically approved for liver cancer treatment.[13] In addition, anionic poly[styrene-*alter*-(maleic acid)] derivatives exhibit low non-specific binding with mammalian cells due to Coulombic repulsion with negatively charged cell surface constituents.[11b, 14] As such, poly[styrene-*alter*-(maleic acid)] $_{40}$, chosen as the carrier, was sequentially amidated with pNIR and 9-amino-9-deoxy-5-N-acetyl-neuraminic acid (9-NH$_2$-SA) in dimethylformamide (Fig. 1). The resultant solution was hydrolyzed with aqueous sodium carbonate solution to abolish residual anhydride, dialyzed over distilled water, and then sonicated to afford nanoscopic pNIR@P@SA by self-assembly. Similarly, poly[styrene-*alter*-(maleic anhydride)]$_{40}$ amidated with pNIR alone was prepared and used as the control (pNIR@P). Dynamic light scattering analysis shows the statistical mean diameters are 86.63 nm and 45.26 nm for pNIR@P@SA and pNIR@P, respectively (Fig. 2), confirming formation of nanoscaled vesicles. Zeta potentials are determined to be -69.0 mv for pNIR@P@SA and -61.5 mv for pNIR@P (ESI†, Fig. S1), which is in consistency with the anionic nature of these polymer vesicles.
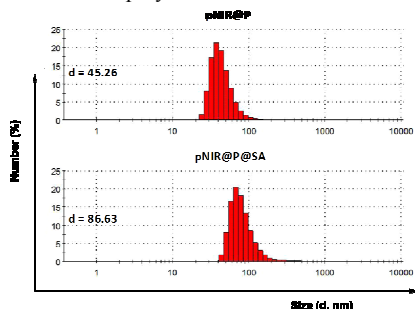


**Fig. 2** Diameters of pNIR@P@SA and pNIR@P measured by dynamic light scattering.

### Acidic pH mediated fluorescence activation of pNIR@P@SA

To ascertain the pH responsiveness, pNIR@P@SA and pNIR@P were respectively spiked into a serial of buffers of pH 4.0-9.0. The solutions were analyzed for UV-Vis-NIR absorption and fluorescence emission as a function of buffer pH.

pNIR@P@SA and pNIR@P displays dramatically enhanced fluorescence emission maximal at 745 nm in acidic buffer (pH 5.5-6.5) relative to alkaline buffer (Fig. 3). Absorption spectra show that both vesicles display absorbance peaked at 720 nm in acidic buffer and intensified as the buffer pH decreases (ESI†, Fig. S2). The spectral analysis validates proton-triggered isomerization of pNIR into NIR-absorbing species (Fig. 1), suggesting the applicability of pNIR-encapsulating vesicles for signal activation based illumination of endo-lysosomes (pH 4.0-6.5) in live cells.
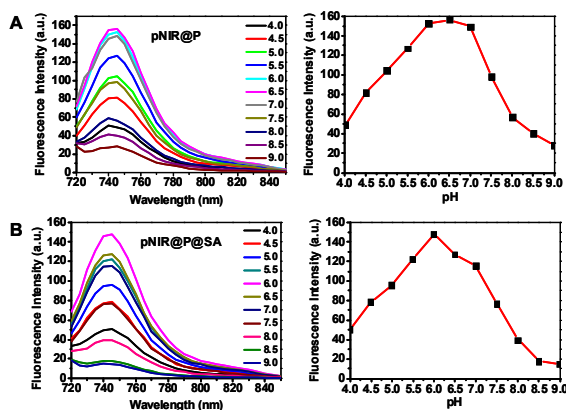


**Fig. 3** pH correlated fluorescence of pNIR@P (A) and pNIR@P@SA (B). The two polymersomes were respectively spiked into sodium phosphate buffer (100 mM, pH 4.0-9.0) to a final concentration of 100 μg ml$^{-1}$. Fluorescence emission of the solutions was recorded using *λex*@715 nm and fluorescence emission intensities@745 nm were plotted over buffer pH.

### Illumination of lysosomes with pNIR@P@SA

Lysosomes are the major constituents of intracellular acidic compartments. We proceeded to investigate lysosome mediated activation of pNIR@P@SA in live cells. HeLa, U87-MG and Raw 264.7 cells were respectively cultured in Dulbecco's Modified Eagle's Medium (DMEM) supplemented with pNIR@P or pNIR@P@SA and then stained with LysoTracker Green DND-26 (referred to as Lysotracker green). As shown in Fig. 4, NIR signals were clearly observed in the three cell lines. Colocalization of NIR fluorescence with Lysotracker green, which is a lysosome-specific dye, reveals that pNIR@P and pNIR@P@SA could be taken up by mammalian cells from culture medium and then delivered into acidic lysosomes.
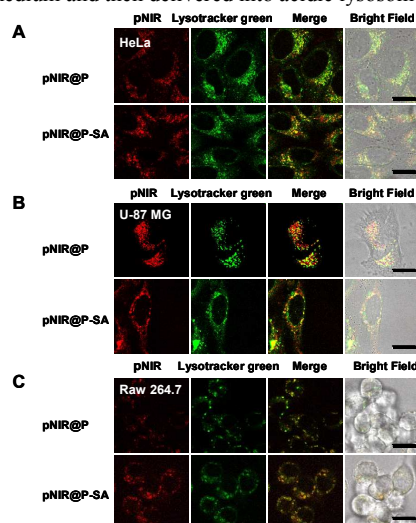


**Fig. 4** Illumination of lysosomes by pNIR@P@SA and pNIR@P.

HeLa (A), U87-MG (B) and Raw 264.7 cells (C) were respectively cultured in DMEM spike with pNIR@P@SA (100 μg ml⁻¹) or pNIR@P (100 μg ml⁻¹) for 1 h. The cells were stained with Lysotracker green (1 μM) in DMEM for 20 min, and then
5 visualized by confocal fluorescence microscopy. Merging of NIR signal (in red) and Lysotracker green (in green) demonstrates colocalization as indicated by the yellow areas. Bars, 10 μm.

To substantiate lysosomal acidity-dependent activation, HeLa
10 cells were first treated with Bafilomycin A1 (BFA), and then co-stained with lysotracker green and pNIR@P@SA or pNIR@P. BFA is a potent ATPase inhibitor and could effectively neutralize lysosomes.[15] The lysosome-specific NIR signals largely vanish in BFA-treated cells (Fig. 5), indicating lysosomal acidity
15 dependent signal activation of internalized vesicles. To ascertain the impact of BFA on vesicle uptake, BFA-treated HeLa cells were incubated pNIR@P@SA or pNIR@P, and then resuspended in sodium phosphate buffer (pH 4.0) for 10 min. Confocal fluorescence microscopic images reveals recovery of bright NIR
20 signals within cells upon suspention in acidic media (Fig. 5), excluding hampered internalization of pNIR@P@SA and pNIR@P into BFA-treated cells. Collectively, these results confirms lysosomal acidity dependent fluorescence activation of endocytosed pNIR@P@SA in live cells. *In vitro* pH titration
25 shows that pNIR@P@SA is strongly fluorescent in acidic medium and yet moderately luminescent in buffer of pH 7.2 (Fig. 3). In contrast, pNIR@P@SA is nearly nonfluorescent in cytosolic pH (pH 7.2) in BFA-treated cells (Fig. 5), which is beneficial for the proposed lysosomal activation based tumor
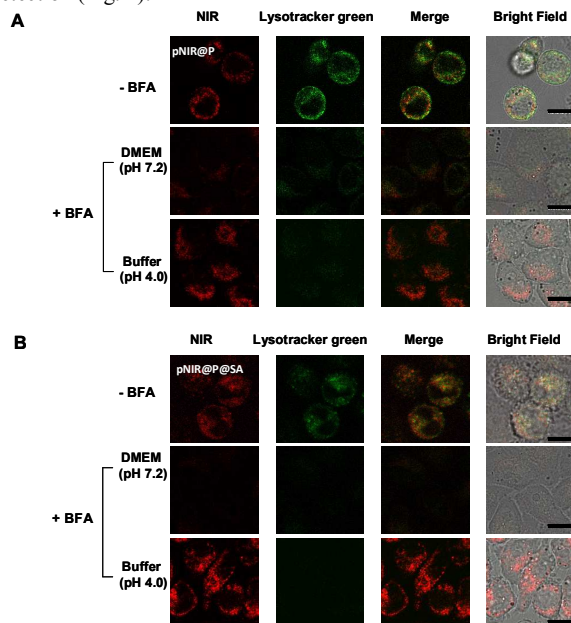30 detection (Fig. 1).



**Fig. 5** Acidity mediated "turn-on" fluorescence of pNIR@P (A) and pNIR@P@SA (B) in live cells. HeLa cells were cultured without or with BFA (100 nM) in DMEM for 4 h, incubated with
35 100 μg ml⁻¹ of pNIR@P or pNIR@P@SA in DMEM for 1 h, and then stained with Lysotracker green (1 μM) in DMEM for 20 min. A portion of the BFA- and vesicle-loaded cells were resuspended in sodium phosphate buffer (pH 4, 100 mM) for 10 min. The cells were visualized by confocal fluorescence microscopy. NIR signal
40 is merged with Lysotracker green and the colocalization is indicated by yellow areas. Bars, 10 μm.

**Fluorescence imaging of subcutaneous tumors in mice with pNIR@P@SA**

Shown to become fluorescent in lysosomes, pNIR@P@SA
45 was evaluated for its efficacy to illuminate subcutaneous tumors in mice. Nude mice were subcutaneously inoculated with H22 hepatocellular carcinoma cells in the flank. The mice were maintained for 5-10 days after inoculation to allow development of H-22 tumor xenografts. pNIR@P@SA and pNIR@P were
50 respectively injected into the tumor-bearing mice *via* tail vein. The mice were imaged for whole body fluorescence at 15 h following injection. Intense NIR signals are clearly identified in subcutaneous tumors in mice treated with pNIR@P@SA whereas moderate NIR signals were detected in subcutaneous tumor
55 treated with pNIR@P at identical doses (Fig. 6A). The mice were sacrificed. The tumors and representative organs were excised and analyzed for *ex vivo* fluorescence emission. Consistent with the whole body imaging results (Fig. 6A), superior tumor-to-healthy organ fluorescence contrasts are identified in the tumors
60 treated with pNIR@P@SA as compared to pNIR@P (Fig. 6B and 6C), validating the superior capacity of pNIR@P@SA to illuminate tumors *in vivo* and the beneficial role of SA displayed on vesicles for enhanced tumor targeting efficiency.
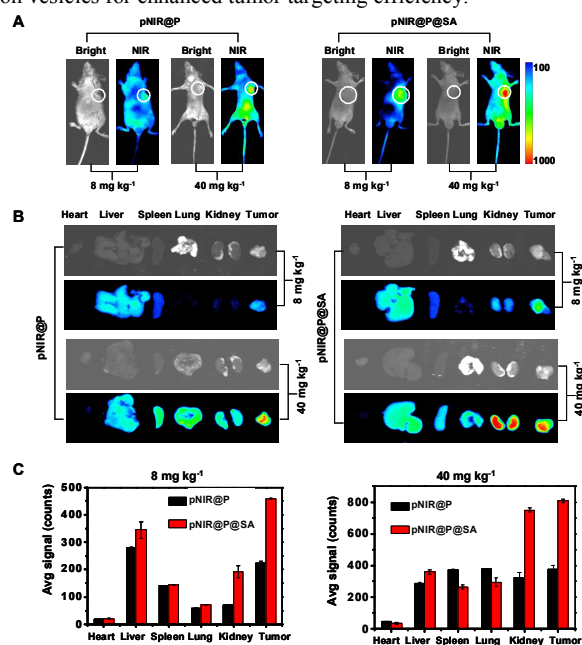


65 **Fig. 6** Superior illumination of subcutaneous tumors with pNIR@P@SA over pNIR@P. Nude mice with subcutaneous H22 tumors were intravenously injected with pNIR@P or pNIR@P@SA (8 mg kg⁻¹ or 40 mg kg⁻¹) *via* tail vein. At 15 h after injection, the mice were imaged for whole body
70 fluorescence (A). The tumor and selected organs harvested from the mice were imaged for *ex vivo* fluorescence (B). The bar graphs show tissue distributions of NIR fluorescence (C). The circles indicate the tumor location.

75 To probe time course of *in vivo* activation of pNIR@P@SA, nude mice bearing subcutaneous H22-tumor xenograft were administered with pNIR@P@SA by tail vein and then monitored for whole body fluorescence at fixed time points. As shown in Fig. 7, NIR signals, negligible in mice up to 30 min after vesicle
80 injection, reach maxima in tumor at 24-48 h and then attenuate at 96 h postinjection. These results verify that pNIR@P@SA is nonfluorescent in blood stream during circulation and then could be internalized and activated by tumors. The long-term retention of high tumor-to-background signal contrast is beneficial for
85 endured practical tumor surgery. The dramatically decreased

whole body NIR signals at 144 h postinjection reveals effective in vivo clearance of pNIR@P@SA (Fig. 7), which is beneficial for *in vivo* biomedical application.
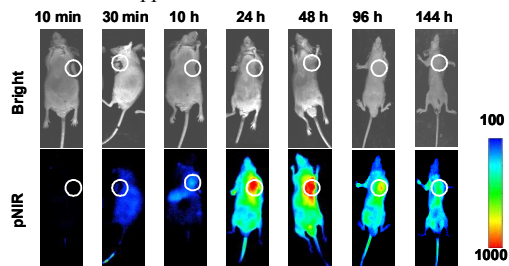


5 **Fig. 7** Time course on whole body fluorescence activation of pNIR@P@SA in tumor-bearing mice. Nude mice bearing H22 subcutaneous tumors were injected by tail vein with pNIR@P@SA (40 mg kg$^{-1}$) and then monitored for whole body fluorescence at 10 min-144 h following vesicle injection. Circles 10 indicate the location of subcutaneous tumors.

**High performance fluorescence imaging of liver tumor foci with pNIR@P@SA**

Hepatocellular carcinoma is a major health problem worldwide with 60,000 new cases diagnosed each year.[16] Surgery combined 15 with chemotherapy remains the primary choice for liver cancer therapy. As such, agents enabling precise detection of liver tumors are of clinical significance. pNIR@P@SA was evaluated for its capacity to illuminate tumor foci in liver. ICR mice with H22 hepatocellular carcinoma implants in liver were injected 20 with pNIR@P@SA or pNIR@P *via* tail vein. At 48 h postinjection, the mice were sacrificed. The tumor-bearing liver and other healthy organs were harvested and subjected to *ex vivo* fluorescence analysis. Intensive NIR signals are indiscriminately distributed in tumor foci and surrounding healthy liver tissue 25 from mice treated with pNIR@P (Fig. 8A). In contrast, high fluorescence contrasts were identified in tumor foci over healthy liver tissue and organs from mice injected with pNIR@P@SA (Fig. 8 B-C).

Hepatocytes efficiently capture and internalize nanoscaled 30 materials,[17] Tumor targeting nanosystems with low levels of hepatic uptake remain challenging. In contrast with the indiscriminate intense fluorescence of pNIR@P in healthy liver tissue and tumor foci, the intense tumor-associated NIR signals and low levels of fluorescence in healthy liver portion further 35 verify the beneficial impacts of SA for *in vivo* tumor uptake (Fig. 8B). The obviously decreased fluorescence intensity of pNIR@P@SA over pNIR@P in the healthy portion of the liver at 48 h (Fig. 8B) postinjection over that at 15 h (Fig. 6B) postinjection shows that pNIR@P@SA displays long term 40 retention in tumor foci whereas pNIR@P@SA in the healthy portion is poised to quick hepatic clearance. Although the cellular machinery or physiological factors responsible for tumor uptake of pNIR@P@SA remains to be elucidated, the results indicate the utility of SA as a tumor targeting ligand.

45 Symptoms of human hepatocellular carcinoma often occur till the tumors grow to 4-8 cm in diameter.[18] A minimum of 1 cm clearance, known as minimal residual disease, is pursued by surgeons during cancer resection.[19] As demonstrated in Fig. 8B, the size of liver tumor discerned by pNIR@P@SA (~4 mm) is 50 significantly below minimal residual cancer (1 cm). The high tumor-to-healthy organ signal contrasts (Fig. 8C) and the capacity to distinguish millimeter-sized liver tumor shows the potentials of SA as a tumor-targeting ligand in nanomedicine.
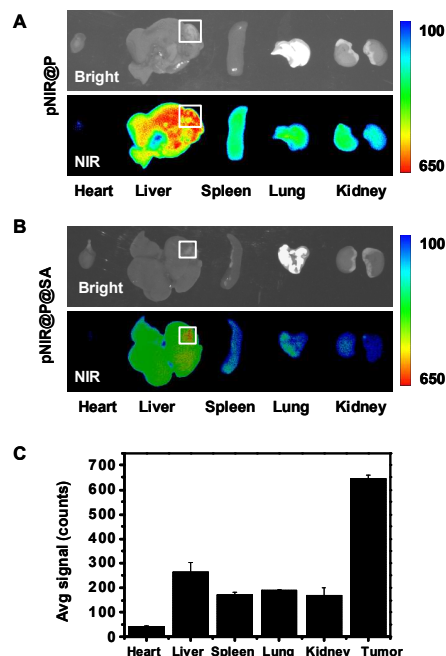


55 **Fig. 8** Illumination of tumor foci in liver with pNIR@P@SA. ICR mice with liver tumor xenografts were intravenously injected with 40 mg kg$^{-1}$ of pNIR@P (A) or pNIR@P@SA (B), and then sacrificed 48 h postinjection. The liver and selected organs were 60 excised and probed for e*x vivo* fluorescence emission. The bar graph shows fluorescence intensity of pNIR@P@SA in tumor foci, healthy liver tissue and other organs as indicated (C). Boxes indicate locations of liver tumor foci.

**Acid activatable photoacoustic property of pNIR@P@SA**

65 Fluorescence imaging suffers from intense photon diffusion within soft tissues whereas acoustic imaging relies on the use of weakly scattered ultrasound and can image objects several centimeters deep in biological tissues.[20] To date, optoacoustic bioimaging has been performed with the aid of exogenous 70 contrast agents such as indocyanine green (ICG), conjugated polymers, and metallic nanoparticles.[21]

Distinct from ICG dye with "always-on" optoacoustic signal, pNIR isomerizes in acidic media to give a NIR fluorophore with strong absorption at 650-750 nm (Fig. 3, and Fig. S2, ESI†). It is 75 anticipatable that a portion of the absorbed optical energy by pNIR at acidic media is released as fluorescence emission and heat as the fluorescence quantum yield is <100%, suggesting the potentials of pNIR as acid activatable optoacousitc agents.

Hence pNIR@P@SA was assessed for acid activatable 80 photoacoustic tumor imaging. Ultrasound is generated from thermoelastic expansion caused by contrast agents excited by pulsed laser. To probe the photothermal effects, the solution containing pNIR@P@SA was exposed to 660-nm laser illumination at the power density of 0.5 W cm$^{-2}$. Time course 85 studies revealed dramatically elevated temperature in the aforementioned solution over probe-free solution (Fig. S3, ESI†), showing the capability of pNIR@P@SA to convert NIR irradiation into heat, proving its photothermal capability. Next, pNIR@P@SA was spiked in to buffer of various pH. The 90 solutions were analyzed for photoacoustic intensity. As shown in Fig. 9, intense PA signals are observed in acidic buffers (pH 6.5-4.5) whereas weak or no signals were identified at neutral to alkaline conditions (pH 7.5-9.5). As SA moiety and the polymeric carrier remained structurally unchanged within pH 4-8, the 95 acidity dependent turn-on optoacoustic contrast of pNIR@P@SA

is clearly due to isomerization of pNIR into fluorescent NIR moiety." To further corroborate this observation, pNIR and the control polymer (P@SA) were assayed for their pH dependent optoacoustic properties underlying optoacoustic imaging. It was shown that pNIR displays acid acitivatble photothermal effects whereas P@SA is innert under identical conditions (Fig. S4). Taken together, these results validats acidic pH mediated "turn-on" optoacoustic signals of pNIR moiety at pNIR@P@SA.
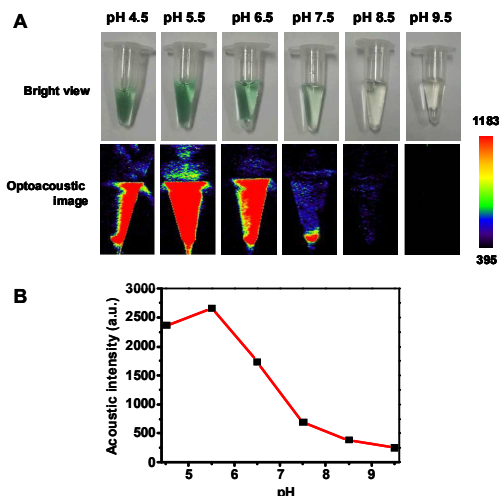


**Fig. 9** Acidic pH mediated activation of photoacoustic property of pNIR@P@SA. pNIR@P@SA was spiked into sodium phosphate buffer (100 mM) of various pH values pH 4.5-9.5) to a final concentration of 1 mg ml$^{-1}$. The solutions were recorded for visual images and photoacoustic contrast (A). The optoacoustic inensity was plotted over buffer pH (B)

### Photoacoustic imaging of tumors in mice with pNIR@P@SA

Nude mice bearing subcutaneous tumors were intravenously injected with pNIR@P@SA or phosphate buffered saline (PBS) and then probed for *in vivo* photoacoustic signals. As shown in Fig. 10, the intratumor vessels can be clearly visualized in intact mice. This observation is consistent with reported optoacoustic imaging of blood vessels.[22] Despite the background optoacoustic contrast resulting from endogenous biomolecules, dramatically increased optoacoustic signals are identified in the tumor from mice following tail vein injection of pNIR@P@SA whereas no variations in optoacoustic brightness are observed in subcutaneous tumor from mice treated with PBS (Fig. 10), proving the applicability of pNIR@P@SA for lysosomal acidity-activatable photoacoustic imaging of tumors. Albeit with limited tissue penetration, NIR fluorescence imaging is of low backgound signals due to minimal biological autofluorescence in NIR region (Fig. 7). Given the obvious optoacoustic contrast intrinsic of physiological constituents (e.g. blood vessel), pNIR@P@SA, with activatable fluorescence and photoacoustic signals, combines the advantages of both acoustic imaging (deep tissue penetration) and NIR fluorescence imaging (low background signals), which is of use for practical intraoperative tumor resection.
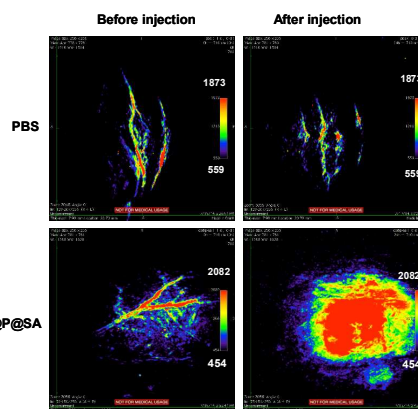


**Fig. 10** Photoacoustic tumor imaging in mice with pNIR@P@SA. Nude mice bearing H22 subcutaneous tumors were intravenously injected with PBS (100 μl) or pNIR@P@SA (40 mg kg$^{-1}$). The mice were imaged 24 h after vesicle injection. Control images were obtained from mice before intravenous injection of pNIR@P@SA or PBS.

### Cytotoxicity of pNIR@P@SA

To probe the cytoxicity of the nanovesicles, HeLa cells were cultured with various levels of pNIR@P@SA or pNIR@P in DMEM. Cell viability were determined by trypan blue exclusion test. No detrimental effects on cell viability were observed at doses up to 100 μg ml$^{-1}$ after 24 h incubation (Fig. 11), indicating that pNIR@P@SA are of low cell toxicity. To ascertain the systemic toxicity, pNIR@P@SA was intravenously injected into mice at doses of to 160 mg kg$^{-1}$ in healthy mice, which is 4 times higher than the doses employed for tumor imaging. The mice were regularly monitored for whole body fluorescence emission and adverse physiological effects after vesicle injection. Whole body fluorescence images of the mice shows that NIR signals, maximal at 4 h postinjection, dramatically decrease over time (Fig. S5, ESI†). The extremely low levels of NIR signals at 7 day postinjection showt high efficiency clearance of injected pNIR@P@SA. In addition, no signs of pain or fatigue could be observed in mice up to 7 days after nanovesicle administration. Poly[styrene-*alter*-(maleic acid)] is biocompatible and has been used as the carrier of neocarcinostation for clinical treatment of primary hepatoma and secondary liver cancer in Japan.[13] Consitently, our results shows that pNIR@P@SA is of low cytotoxicity and systemic toxicity, which are critical for *in vivo* imaging studies.
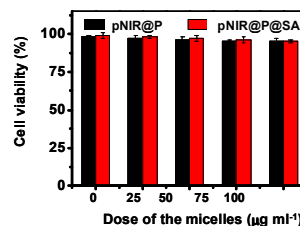


**Fig. 11** Cytotoxicity of pNIR@P@SA and pNIR@P. HeLa cells were cultured for 24 h in DMEM spiked with various amounts of pNIR@P or pNIR@P@SA (0, 25, 50, 100 μg ml$^{-1}$). The cell number and cell viability were determined by trypan blue exclusion.

## Conclusion

We demonstrate the use of a multifunctional nanovesicle for signal activation based fluorescence and photoacoustic tumor imaging in mice. The naonovesicle, pNIR@P@SA, consists of

surface-anchored sialic acid for tumor targeting, a biocompatible carrier of poly[styrene-*alter*-(maleic acid)], and a core of near infrared profluorophore poised to proton triggered isomerization to give NIR fluorescence and optoacoustic signals in lysosomes. pNIR@P@SA effectively illuminates subcutaneous tumor and millimeter-sized tumor foci in liver with high target-to-healthy organ signal contrasts, validating the potential of sialic acid as a tumor targeting ligand in nanomedicine. The distinguished tumor-associated fluorescence and acoustic contrasts demonstrate the applicability of pNIR@P@SA for dual modality tumor imaging. Integrating the advantages of NIR fluorescence (low background) and optoacoustic imaging (deep tissue penetration), this activatable nanosystem, readily modulated for imaging of different tumors by incorporation of cognate targeting entities on vesicle surface, would be of broad interests for dual modality cancer diagnosis and imaging guided tumor surgery.

State Key Laboratory for Physical Chemistry of Solid Surfaces

## Notes and references

*aState Key Laboratory for Physical Chemistry of Solid Surfaces, the Key Laboratory for Chemical Biology of Fujian Province, The MOE Key Laboratory of Spectrochemical Analysis & Instrumentation, Innovation Center for Cell Biology, and Department of Chemical Biology, College of Chemistry and Chemical Engineering Xiamen University; bState key Laboratory of Cellular Stress Biology, Innovation Center for Cell Biology, School of Life Sciences, Xiamen University, Xiamen, 361005, China; Tel: 86-0592-2181728; E-mail: shoufa@xmu.edu.cn*

† Electronic Supplementary Information (ESI) available on experimental procedures; See DOI: 10.1039/b000000x/

1 (a) Y. Urano, M. Sakabe, N. Kosaka, M. Ogawa, M. Mitsunaga, D. Asanuma, M. Kamiya, M. R. Young, T. Nagano, P. L. Choyke, H. Kobayashi, *Sci. Transl. Med.,* 2011, **3**, 110ra119; (b) Q. T. Nguyen, E. S. Olson, T. A. Aguilera, T. Jiang, M. Scadeng, L. G. Ellies, R. Y. Tsien, *Proc. Natl. Acad. Sci. USA.,* 2010, **107**, 4317; (c) Y. Urano, D. Asanuma, Y. Hama, Y. Koyama, T. Barrett, M. Kamiya, T. Nagano, T. Watanabe, A. Hasegawa, P. L. Choyke, H. Kobayashi, *Nat. Med.,* 2009, **15**, 104; (d) S. L. Troyan, V. Kianzad, S. L. Gibbs-Strauss, S. Gioux, A. Matsui, R. Oketokoun, L. Ngo, A. Khamene, F. Azar, J. V. Frangioni, *Ann. Surg. Oncol.,* 2009, **16**, 2943; (e) Q. T. Nguyen, R. Y. Tsien, *Nat. Rev. Cancer,* 2013, **13**, 653.

2 (a) H. Kobayashi, P. L. Choyke, *Acc. Chem. Res.,* 2011, **44**, 83; (b) K. Sokolov, D. Nida, M. Descour, A. Lacy, M. Levy, B. Hall, S. Dharmawardhane, A. Ellington, B. Korgel, R. Richards-Kortum, *Adv. Cancer Res.,* 2007, **96**, 299; (c) G. M. van Dam, G. Themelis, L. M. Crane, N. J. Harlaar, R. G. Pleijhuis, W. Kelder, A. Sarantopoulos, J. S. de Jong, H. J. Arts, A. G. van der Zee, J. Bart, P. S. Low, V. Ntziachristos, *Nat. Med.,* 2011, **17**, 1315.

3 (a) T. Angata, A. Varki, *Chem. Rev.,* 2002, **102**, 439; (b) B. E. Collins, J. C. Paulson, *Curr. Opin. Chem. Biol.,* 2004, **8**, 617; (c) Y. Pilatte, J. Bignon, C. R. Lambre, *Glycobiology,* 1993, **3**, 201; (d) T. A. Springer, *Cell,* 1994, **76**, 301.

4 (a) S. Hakomori, *Cancer Res.,* 1996, **56**, 5309; (b) R. Kannagi, K. Sakuma, K. Miyazaki, K. T. Lim, A. Yusa, J. Yin, M. Izawa, *Cancer Sci.,* 2010, **101**, 586; (c) Y. Xu, A. Sette, J. Sidney, S. J. Gendler, A. Franco, *Immunol. Cell Biol.,* 2005, **83**, 440.

5 (a) X. Wu, Y. Tian, B. Lin, J. Han, S. Han, *Biomater. Sci.,* 2014, **2**, 1120; (b) X. Wu, B. Lin, M. Yu, H. Xing, J. Han, S. Han, *Chem. Sci.,* 2015, DOI: 10.1039/C4SC02248C.

6 (a) L. V. Wang, S. Hu, *Science,* 2012, **335**, 1458; (b) L. Nie, X. Chen, *Chem. Soc. Rev.,* 2014, DOI: 10.1039/C4CS00086B; (c) K. Li, B. Liu, *Chem. Soc. Rev.,* 2014, DOI: 10.1039/C4CS00014E

7 (a) K. Pu, A. J. Shuhendler, J. V. Jokerst, J. Mei, S. S. Gambhir, Z. Bao, J. Rao, *Nat. Nanotechnol.,* 2014, **9**, 233; (b) J. Levi, S. R. Kothapalli, T. J. Ma, K. Hartman, B. T. Khuri-Yakub, S. S. Gambhir, *J. Am. Chem. Soc.,* 2010, **132**, 11264.

8 (a) H. Kouyoumdjian, D. C. Zhu, M. H. El-Dakdouki, K. Lorenz, J. Chen, W. Li, X. Huang, *ACS Chem. Neurosci.,* 2013, **4**, 575; (b) J. E. Hudak, S. M. Canham, C. R. Bertozzi, *Nat. Chem. Biol.,* 2014, **10**, 69; (c) A. Nazemi, S. M. Haeryfar, E. R. Gillies, *Langmuir,* 2013, **29**, 6420; (d) J. Minaguchi, T. Oohashi, K. Inagawa, A. Ohtsuka, Y. Ninomiya, *Arch. Histol. Cytol.,* 2008, **71**, 195; (e) N. Hashida, N. Ohguro, N. Yamazaki, Y. Arakawa, E. Oiki, H. Mashimo, N. Kurokawa, Y. Tano, *Exp. Eye. Res.,* 2008, **86**, 138; (f) L. Bondioli, L. Costantino, A. Ballestrazzi, D. Lucchesi, D. Boraschi, F. Pellati, S. Benvenuti, G. Tosi, M. A. Vandelli, *Biomaterials,* 2010, **31**, 3395; (g) K. Totani, T. Kubota, T. Kuroda, T. Murata, K. I. Hidari, T. Suzuki, Y. Suzuki, K. Kobayashi, H. Ashida, K. Yamamoto, T. Usui, *Glycobiology,* 2003, **13**, 315; (h) I. Papp, C. Sieben, K. Ludwig, M. Roskamp, C. Bottcher, S. Schlecht, A. Herrmann, R. Haag, *Small,* 2010, **6**, 2900.

9 P. R. Crocker, J. C. Paulson, A. Varki, *Nat. Rev. Immunol.,* 2007, **7**, 255.

10 H. Kobayashi, M. Ogawa, R. Alford, P. L. Choyke, Y. Urano, *Chem. Rev.,* 2010, **110**, 2620.

11 (a) X. Wu, Y. Tian, M. Yu, J. Han, S. Han, *Biomater. Sci.,* 2014, **2**, 972; (b) Z. Li, Y. Song, Y. Yang, L. Yang, X. Huang, J. Han, S. Han, *Chem. Sci.,* 2012, **3**, 2941.

12 R. Weissleder, V. Ntziachristos, *Nat. Med.,* 2003, **9**, 123.

13 A. K. Iyer, G. Khaled, J. Fang, H. Maeda, *Drug Discov. Today,* 2006, **11**, 812.

14 L. Yang, S. Wu, B. Lin, X. Chen, S. Han, *J. Mater. Chem. B,* 2013, **1**, 6115.

15 T. Yoshimori, A. Yamamoto, Y. Moriyama, Y. Futai, Y. Tashiro, *J. Biol. Chem.,* 1991, **266**, 17707.

16 (a) P. Ferenci, M. Fried, D. Labrecque, J. Bruix, M. Sherman, M. Omata, J. Heathcote, T. Piratsivuth, M. Kew, J. A. Otegbayo, S. S. Zheng, S. Sarin, S. S. Hamid, S. B. Modawi, W. Fleig, S. Fedail, A. Thomson, P. Malfertheiner, G. Lau, F. J. Carillo, J. Krabshuis, A. Le Mair, *J. Clin. Gastroenterol.,* 2010, **44**, 239; (b) Y. Kim do, K. H. Han, *Liver Cancer,* 2012, **1**, 2; (c) M. Sherman, *Semin. Liver Dis.,* 2010, 30, 3.

17 (a) T. Kasuya, S. Kuroda, *Expert Opin. Drug Deliv.,* 2009, **6**, 39; (b) J. D. Perkins, *Liver Transpl.,* 2007, **13**, 167.

18 (a) F. Trevisani, M. C. Cantarini, J. R. Wands, M. Bernardi, *Carcinogenesis,* 2008, **29**, 1299; (b) M. Colombo, *J. Hepatol.,* 1992, **15**, 225.

19 (a) M. Partridge, S. R. Li, S. Pateromichelakis, R. Francis, E. Phillips, X. H. Huang, F. Tesfa-Selase, J. D. Langdon, *Clin. Cancer Res.,* 2000, **6**, 2718; (b) K. Pantel, T. J. Moss, *Cytotherapy,* 1999, 53.

20 (a) E. I. Galanzha, E. V. Shashkov, T. Kelly, J. W. Kim, L. Yang, V. P. Zharov, *Nat. Nanotechnol.,* 2009, **4**, 855; (b) L. Li, K. Maslov, G. Ku, L. V. Wang, *Opt. Express,* 2009, **17**, 16450.

21 (a) M. Chen, X. Fang, S. Tang, N. Zheng, *Chem. Commun.,* 2012, **48**, 8934; (b) X. Xia, M. Yang, L. K. Oetjen, Y. Zhang, Q. Li, J. Chen, Y. Xia, *Nano. Lett.,* 2011, **3**, 950; (c) L. Nie, M. Chen, X. Sun, P. Rong, N. Zheng, X. Chen, *Nanoscale,* 2014, **6**, 1271; (d) Z. Zha, Z. Deng, Y. Li, C. Li, J. Wang, S. Wang, E. Qu, Z. Dai, *Nanoscale,* 2013, **5**, 4462; (e) A. Hannah, G. Luke, K. Wilson, K. Homan, S. Emelianov, *ACS Nano.,* 2014, **8**, 250; (f) G. Kim, S. W. Huang, K. C. Day, M. O'Donnell, R. R. Agayan, M. A. Day, R. Kopelman, S. Ashkenazi, *J. Biomed. Opt.,* 2007, **12**, 044020; (g) C. Xu, P. D. Kumavor, U. Alqasemi, H. Li, Y. Xu, S. Zaganeh, Q. Zhu, *J. Biomed. Opt.,* 2013, **18**, 126006; (h) S. Zaganeh, H. Li, P. D. Kumavor, U. Alqasemi, A. Aguirre, I. Mohammad, C. Stanford, M. B. Smith, Q. Zhu, *J. Biomed. Opt.,* 2013, **18**, 096006; (i) J. Zhong, S. Yang, X. Zheng, T. Zhou, D. Xing, *Nanomedicine,* 2013, **8**, 903.

22 (a) H. P. Brecht, R. Su, M. Fronheiser, S. A. Ermilov, A. Conjusteau, A. A. Oraevsky, *J. Biomed. Opt.,* 2009, **14**, 064007; (b) K. Wang, S. A. Ermilov, R. Su, H. P. Brecht, A. A. Oraevsky, M. A. Anastasio, *IEEE Trans. Med. Imaging,* 2011, **30**, 203.